EFDA–JET–PR(07)64

K.K. Kirov, M-L. Mayoral, J. Mailloux, Yu. Baranov, L. Colas, A. Ekedahl, K. Erents, M. Goniche, P. Jacquet, A. Korotkov, P. Morgan, V. Petrzilka, J. Ongena, K. Rantamäki, M. Stamp and JET EFDA contributors

LH Wave Coupling and ICRF Induced Density Modifications At JET

LH Wave Coupling and ICRF Induced Density Modifications At JET

K. K. Kirov[1], M-L. Mayoral[1], J. Mailloux[1], Yu. Baranov[1], L. Colas[2], A. Ekedahl[2], K. Erents[1], M. Goniche[2], P. Jacquet[1], A. Korotkov[1], P. Morgan[1], V. Petrzilka[3], J. Ongena[4], K. Rantamäki[5], M. Stamp[1] and JET EFDA contributors*

JET-EFDA, Culham Science Centre, OX14 3DB, Abingdon, UK

[1]EURATOM-UKAEA Fusion Association, Culham Science Centre, OX14 3DB, Abingdon, OXON, UK
[2]Association EURATOM-CEA, 13108 St Paul-lez-Durance, France
[3]Association EURATOM/IPP.CR, Prague, Czech Republic
[4]Plasmaphysics Lab, ERM-KMS, Association EURATOM-Belgian State, Brussels, Belgium
[5]Association EURATOM-Tekes, VTT, Espoo, Finland
** See annex of M.L. Watkins et al, "Overview of JET Results ",*
(Proc. 21 st IAEA Fusion Energy Conference, Chengdu, China (2006)).

Preprint of Paper to be submitted for publication in
Nuclear Fusion

ABSTRACT.
Lower Hybrid (LH) wave coupling is modified and usually degraded when the system is powered simultaneously with Ion Cyclotron Range of Frequencies (ICRF) antennas magnetically connected to the launcher. This has been attributed to Scrape-Off Layer (SOL) density modifications by the RF sheaths. LH Reflection Coefficients dependencies on various parameters are investigated and shown to be consistent with RF sheath physics. Gas puffing near the launcher has been used to improve the coupling of LH waves.

1. INTRODUCTION

Lower Hybrid Current Drive (LHCD) is the most efficient way to generate non-inductive current in a fusion plasma. It is beneficial not only for the overall plasma operation, in particular achieving very long pulse duration [1], but also provides an efficient way of shaping the current profile and slowing down the plasma current diffusion. In JET Lower Hybrid (LH) power is usually applied in the early phase of the discharge during the current ramp-up phase, driving off-axis co-current, resulting in weak negative or flat magnetic shear, which favours the formation of Internal Transport Barriers (ITBs) [2], [3]. LHCD is also applied during the main heating phase to sustain and prolong its duration.

Achieving good coupling of the slow wave, associated with the LH wave, can be however, a very challenging task. Early studies [4] have demonstrated a robust way of launching plasma waves in the LH range of frequencies by utilisation of a multi-waveguide launching structure, or grill, which consists of an array of open-ended radiating waveguides. Detailed investigations [4], [5] have shown that the coupling, measured by the amount of microwave power injected into the plasma, is strongly related to the density in front of the launcher. Therefore, the LH coupling performance will depend on all the processes, which affect the edge plasma density such as the gas puffing and recycling, H-mode edge barrier and ELMs, edge turbulence phenomena and modifications by the heating systems. The latter includes the RF generated sheaths and their impact on the particle transport in the Scrape-Off Layer (SOL). The complexity and the mutual dependence of all these processes make the full theoretical treatment of the problem very difficult. However, experimental studies aiming at achieving good coupling and optimisation of the LHCD performance provide valuable information to get a better understanding of the problem.

The LH launcher at JET is situated near the ICRF antenna B. It is magnetically connected to ICRF antenna B for all plasma operations and for some plasma scenarios also to ICRF antenna A. Antenna B was rarely pulsed simultaneously with LHCD before 2004 due to its detrimental effect on the LH coupling demonstrated in experiments [6]. Since 2005, antennas A and B are powered by the same generators and turning them off would result in severe power limitation for experiments requiring LHCD and ICRF power. This motivated experiments in 2006 to continue to investigate the effect of ICRF antennas B and A on LH coupling, and try to improve it.

Understanding the effect of ICRF generated SOL density modifications on LH wave coupling is an important issue regarding (*i*) the optimisation of the performance of the LHCD system at JET and (*ii*) the decision on the LHCD port allocation for ITER and the related implications. JET features both heating systems and the forthcoming installation of the ITER-like antenna makes it therefore

a unique device for studying their mutual operation in ITER relevant conditions.

The effect of Ion Cyclotron Radio Frequency (ICRF) heating on LH wave coupling has been studied and documented on Tore Supra and has been attributed to the RF sheaths [6], [7], [8]. Similar experimental investigations have been performed at JET [6], [9], [10], where LH coupling has been shown to deteriorate when ICRF antennas B and A are used. A density pump out effect in front of the ICRF antennas was observed experimentally in TFTR [11] as well.

This paper summarises the recent results from the LH coupling studies in presence of RF sheaths. Experimental results will be highlighted and the conclusions will be based on the coupling results from particular experiments. The paper is organised as follows. A description of the LHCD and ICRF systems and the utilised diagnostics is given in section 2. The various aspects of the LH coupling and the physics of RF sheaths are briefly discussed in section 3. The experimental results showing the important parametric dependencies are presented in section 4. Section 5 highlights the most important conclusions.

2. IN-VESSEL LAYOUT OF THE INVESTIGATED HEATING SYSTEMS

The LHCD launcher and the ICRF antenna B are shown in figure 1 and drawings of the toroidal and the poloidal geometry of the vessel are given in figure 2. In order to avoid confusion the word 'antenna' will be exclusively used to denote the ICRF coupling structure, while the one used to couple the LH waves will be referred to as a 'LHCD launcher'.

The LHCD system at JET consists of 24 klystrons, each of which is capable to generate up to 500kW at 3.7GHz for pulses of up to 20s or alternatively 650kW for 10s. [12]. The klystrons are arranged in 6 modules (named A to F) for control and protection purposes. Each klystron feeds two hybrid junctions, ordered in 6 rows and 8 columns at the launcher mouth and each hybrid junction is further split into 4-rows-by-2-columns section by *E*- and *H*-plane multijunctions. In the experiments presented here the LH wave was launched with $N_{||} = 1.8$, which can be achieved at 0^{o} phasing between the multijunctions. When LHCD is pulsed, often not all the klystrons are available. Also in most of the cases they deliver different amounts of power. The Reflection Coefficients (RCs) slightly depend on the power generated by the energised klystrons therefore supplementary information on this contribution will be provided in the study.

The launcher as seen from inside the torus, figure 1, consists of a grill and a surrounding protection frame. On the left hand side of the launcher there is a gas pipe, Gas Injection Module 6 (GIM6), and a Poloidal Limiter (PL) further away in Oct. 4. The ICRF antenna B is on the right hand side of the LHCD launcher. The launcher and the antenna are separated by a narrow poloidal limiter (nPL), which is radially -0.005m, figure 2c, behind the other poloidal limiters. The ICRF antenna B, similarly to all the other JET A2 ICRF antennas, comprises four straps (e.g. for antenna B they are named B1, B2, B3 and B4) which are powered by separate generators and can be phased independently. By changing the phase shift between different straps the fast wave can be coupled in monopole $(0, 0, 0, 0)$, dipole $(0, \pi, 0, \pi)$ or asymmetric spectra $+\pi/2$ $(0, \pi/2, \pi, 3\pi/2)$ or $-\pi/2$ $(0, -\pi/2, -\pi, -3\pi/2)$, where the numbers in the brackets indicate the relative phase of straps 1 to 4. The pairs B1-B2 and B3-B4 can be energised independently and are separated by the RF septum. The latter is in the shadow of the PL and has approximately the same curvature profile as the nPL.

Each strap is equipped with its own Faraday Screen (FS), which is about -0.018m behind the PL. ICRF antenna A is further away, in Oct. 2, separated from antenna B by two limiters. Magnetic field line traces in front of the LHCD launcher are given for three cases of interest, $q_{95} = 4.2$ (2.6T/2MA) dashed lines in figure 2a, $q_{95} = 5.8$ (2.6T/1.5MA) dash-dot lines and $q_{95} = 4.4$ (2.9T/2.2MA) solid line in figure 2b. In some configurations with small q_{95} the top part of antenna A is connected to the bottom half of the launcher, as in figure 2a, while at larger q_{95} the grill is almost fully connected to it, as in figure 2b. As a result, differences between antenna A, straps B1-B2 and B3-B4 on the LH coupling are expected.

The poloidal cross section in figure 2c shows the geometry of the limiters and the antennas and also displays the parameters Radius of the Outer Gap (ROG), r_{ROG}, which is the distance between the separatrix and the PL, and launcher position relative to nPL, l_{pos}. The alignment of the components and the typical values of r_{ROG} and l_{pos} are given as well. A top vessel view as a cut at the midplane is shown in figure 2d. The plasma current I_{p} and magnetic field B_{t} are in clockwise direction in this plot.

Two diagnostics have been utilised in the study to measure the SOL density profiles, so a brief description of them, the Reciprocating Probe (RCP) and the Li beam diagnostic is given here. The RCP probe is located on the top of the vessel in Oct. 5, figure 2b and figure 2d. In the configurations used here the RCP probe is connected to antenna A and to the bottom part of antenna B, an example magnetic field line is shown by solid line in figure 2b. The probe [13] comprises five pins, one of which is a Langmuir probe and sweeps the voltage in the range +50V to –200V. At high ICRF power, larger than 2.5MW, the floating potential becomes significantly affected, negatively biased, by the rectified RF sheath potential [14] thus the ion saturation current, J_{sat}, measurements are spoiled and with large error bars. However, providing the ICRF power does not exceed 2.5MW then in favourable plasma conditions the RCP probe, equipped with high frequency filters, can be used successfully to measure the SOL density profiles [15]. The error bars of the SOL density are however large as they incorporate the uncertainties in J_{sat} measurements and SOL electron temperature measurements. The latter is affected by the RF sheaths as well.

The edge density profiles obtained by the Li beam diagnostic are mostly used in this study. The beam injector in JET [16] provides 0.5-1mA of equivalent neutral current at energy of the Li atoms 50-70keV. It is situated on the top of the vessel in Oct. 7. The beam is directed vertically downward at R=3.25m and a periscope looks orthogonal to the beam line, figure 2d. The optical system measures the whole emission profile of the transition 2p-2s at 670.8nm, which is used for the edge density profiles determination. The latter is possible as the Li atoms feature a weak dependence of the excitation and ionisation rate coefficients on the electron temperature at the conditions of interest. The diagnostic provides very reliable measurements; error bars are estimated to be smaller than 5% in the gradient area. The errors in the spatial location of the profiles are determined by the equilibrium reconstruction inaccuracy, which is estimated to be about 0.01-0.02m. The spatial inaccuracy can be, however, eliminated providing the profiles used for comparison are taken during steady state plasma configuration. The precision in these conditions is estimated smaller than 0.002m.

The LH coupling with ICRF antenna B was investigated in two experimental campaigns. The first one was in 2002 and studied the effect of the ICRF power and plasma configuration on the LHCD performance. The second one was in 2006 and focused more on finding a solution for mutual operation of both systems by means of D_2 gas puff from GIM6 rather than a complete investigation of the problem. Data from experiments, when both systems were used are analysed as well.

3. LH COUPLING AND THE IMPACT OF THE RF SHEATHS

As the conclusions of the study will be based mainly on the reflection coefficient measurements, their derivation and an account of the possible discrepancies and errors in their interpretation is given here.

3.1. LH COUPLING AND REFLECTION COEFFICIENTS

In general the coupling of LH waves depends on the electron density in front of the grill. The slow wave can not propagate at densities lower than the cut-off density, $n_{e,cutoff}$, about $1.7\times10^{17}m^{-3}$ for waves at 3.7GHz, meaning that one should provide $n_e>n_{e,cutoff}$ in front of the launcher mouth for good coupling. However, even if this condition is not fulfilled assuming the region with depleted density, $n_e<n_{e,cutoff}$, is thin enough the wave can still be launched as tunnelling through the SOL is possible. Depending on the width of the gap between the launcher and the position at which $n_e=n_{e,cutoff}$, and to a smaller extent on the density gradient, some amount of the forward wave will be reflected back to the launcher. The LHCD launcher is a phased array antenna thus the reflected wave will be directed not only to the energised waveguides but a substantial amount of it will also be scattered to the adjacent ones. Therefore, cross coupling between adjacent multijunctions, fed by different klystrons, can occur within a row but the influence between different rows is considered negligible.

The RCs are computed as an average over a particular row, i.e. row #1 to #6, according to the formula:

$$RC\#n = \frac{\sum_{m=1}^{8} P_{r,nm}}{0.92\times\sum_{m=1}^{8} P_{f,nm}}, n=1,\ldots,6$$

where n is the row number, $P_{r,nm}$ and $P_{f,nm}$ are the reflected and the forward powers on the n-th row, m-th column multijunction. The forward power $P_{f,nm}$ is taken as a half of the power generated by the corresponding klystron, measurements are taken near the output of each klystron, and the factor 0.92 accounts for the transmission line losses.

The reflected power is measured individually at each multijunction by means of directional couplers, situated just at the back of the launcher, and RF cables carrying the attenuated RF signal to the crystal detectors with an associated electronic circuit to linearise the signal. These components are calibrated after each shutdown, however, small changes in the calibration factors and possible slow variations in the characteristics of the microwave components, including the cables and the connectors, can also affect the accuracy of the RCs calculation. Two types of errors in LH reflected power measurements are considered here: systematic and random. The systematic ones account for:

(*i*) difference in the test equipment used for calibration and changes in the cables and directional couplers attenuation over the years; and (*ii*) inaccuracy in calibration factors determination. These contributions are expected to have impact when comparing the RCs of recent and past experiments. It is impossible to determine the cause of systematic error (*i*), however, analysis of the documented changes over the last five years show that they will result in inaccuracy smaller than 25% in RCs. The detectors and electronic circuits were calibrated in 2006 over the range of reflected power between 0kW to 100kW, so that all the data from the new experimental campaigns, i.e. from JET Pulse No: 64640 onward, were re-processed meaning that for these pulses systematic error (*ii*) is removed. The full calibration curves were not available before 2006. However, similar calibration factors are expected since the diodes and electronics, and the calibration method, were the same. Based on this, it is assessed that in the range of reflected powers observed the lack of the full calibration curves before 2006 resulted in about 20% smaller RCs values for the earlier pulses.

In order to minimise the effect of the systematic errors on the analysis, we only consider relative RC changes. In addition, only data taken over short periods of time, usually in the same experimental session, are used for comparison. This approach minimizes significantly the impact of the systematic errors on the conclusions in the paper. The RC measurements are also averaged during steady state conditions in time intervals between 0.05s to 0.5s. Only the random errors are considered, the error bars shown here are related to the RCs variations during their measurement.

Slightly different RCs are observed when different parts of the launcher are powered. In some cases we observe more reflected power on some parts of the grill and less on others. This can be related to the non-perfect launcher geometry, e.g. caused by the poloidal and toroidal shaping of the launcher and in particular by the damage to the top left corner of the grill. The RCs are affected by the trips of the launcher protection system as well. This is because the cross-coupling between multijunctions on one row changes if some of the klystrons power on that row are turned off. The protection system compares the reflected powers from the upper and the bottom multijunctions corresponding to each klystron and turns its power off if their ratio exceeds a set level, because a very low or very high ratio could indicate that an arc is taking place at the grill mouth or inside the waveguides. The protection system stops the corresponding klystron for about 0.1s after which time the power is reapplied. If the conditions have not improved the klystron is stopped again for 0.1s. When the coupling conditions are bad, the reflected powers are high and get near the threshold of operation of the protection system. Also, the imbalance in the reflected powers is usually larger. Hence many trips are observed in these conditions, and this results in very 'ragged' waveforms, which affects not only the overall LHCD performance but also the RCs.

An example illustrating the importance of all contributions discussed here is given in figure 3, where the RCs measurements within the investigated time interval are shown as statistical boxplots. The boxes and the whiskers present the range of the most likely data. The outliers are the data that deviate significantly from the rest of the data points and in general the larger their number is the more inaccurate the measurement is. During the pulse shown in figure 3 the plasma configuration and the SOL parameters were kept constant between 21s and 25s, meaning that the RCs on rows #3 and #4 should be constant. However, as in time interval TS1 three klystrons were tripping the RCs have many

wide spread outliers, while in case TS2 when none of the klystrons was tripping the RCs are steady, reliable and not scattered. As a result of the tripping the average values of the RCs during TS1, 0.16 for RC #3 and 0.09 for RC #4, are shifted towards the outliers and differ from the TS2 values, 0.14 for RC #3 and 0.08 for RC #4. When one of the klystrons is turned off, C3 in case TS3, the RCs are higher, 0.16 for RC #3 and 0.1 for RC #4, which emphasises the necessity of observing unchangeable klystron configuration when analysing the LH wave coupling.

The multidimensionality of the problem and the complex dependency of the LH RCs on the SOL parameters, plasma configuration and the wave heating systems complicates significantly the analysis of the data. In order to investigate the effect of a particular parameter on the LH wave coupling we select experiments in which only this parameter is varied while all the other contributions are fixed. The comparison of the RCs will be done by observing the following conditions:

- Non tripping cases will be investigated only;
- Same power levels from the klystrons, same klystron configuration, i.e. cases with similar patterns of the powered klystrons;
- Conclusions will be based on comparison of the RCs in steady state and similar plasma conditions: launcher position relative to nPL l_{pos}, separatrix – PL distance at the midplane r_{ROG}, safety factor near the separatrix q_{95} (or alternatively the plasma current I_p and the magnetic field B_t), electron density n_e, gas injection rate from GIM6, G06R, LH coupled power P_{LH}, recycling rate measured by the $D\alpha$ intensity and the plasma configuration including the elongation ε, the upper δ_u and the lower triangularity δ_l.

4. RF SHEATHS

The RF sheaths effects are thoroughly investigated and there is a substantial number of sources in the literature, [7], [17], [18], [19], [20], [21], [22]. Here only a brief description of this phenomenon will be given, and the ICRF related parameters, that are expected to affect the LH wave coupling will be highlighted.

The RF sheaths are caused by interactions of the plasma with the surrounding materials close to powered ICRF antennas. RF electric field along the magnetic field lines develops due to the non-perfect alignment between the latter and the Faraday Screen (FS) bars. Rectified sheath potential can build up at the surface boundaries, e.g. Faraday Screen, septum, limiters due to this field. The sheath has a spatial structure determined by the dimensions of the antenna, e.g. FS screen bars, size of the straps, etc., and the gradients of the sheath potential give rise to $E \times B$ drift and so called RF induced convective cells, which can locally modify the SOL density. The latter is responsible for enhanced transport in the SOL resulting in density redistribution in front of the ICRF antenna and the nearby components.

Various models and a number of results from numerical simulations exist for the RF sheaths. The computation of the sheath potential requires precise knowledge of the antenna geometry and dimensions. The full wave code with 3D antenna, ICANT, was used to compute the sheath topology in front of Tore Supra ICRF antennas [23]. The sheath potential from that code was also used to compute the density depletion in front of the antenna caused by $E \times B$ drift [7].

The rectified sheath potential is shown to scale with square root of the applied ICRF power.

Earlier 1-D models [17], [22] assuming small Larmor radius magnetised ions yielded shield scaling independent of the magnetic field line inclination. The ion demagnetisation case [21] was treated as well, while more recent studies [20] use convective cell treatment to explain the different behaviour of the H-mode edge barrier when using monopole and dipole ICRF power. The ICRF antenna phasing is found to have a strong impact on the SOL plasma as on JET ICRF antennas the monopole phasing will result [24] in about two to three times higher RF sheath voltage compared to dipole phasing.

The RF sheaths do not affect directly the LH wave coupling in JET as the launcher and the ICRF antenna B are separated by a poloidal limiter. In typical JET conditions, $n_{e,SOL} \approx 1 \times 10^{17} m^{-3}$ at the antenna private SOL, the plasma skin depth is estimated to be $\delta \approx 0.016$m, meaning that at the front of the limiter the RF field will be reduced more than twice. Taking into account that the launcher is behind the nPL it can be concluded that the effect of the ICRF on the LH coupling is through RF sheaths modifications of the SOL density in front of the limiter.

The effect of the RF sheaths on the SOL density can be demonstrated by means of SOL density measurements. The Li beam profiles are taken so that the densities inside the separatrix are comparable. Similar plasma parameters, e.g. plasma shape and core plasma density, were observed as well, whilst the configuration was selected so that the powered ICRF antennas were magnetically connected to the diagnostic port. The edge density profile during a 2MW ICRF pulse is compared to the no power reference in figure 4a. The application of RF power clearly depletes the electron density in the region from 3.85m to about 3.9m. The decrease is estimated between 30% near the separatrix and 60% for the most outer points. In figure 4b the Li beam data are shown for two cases, in which 2.5MW of ICRF power was applied first in dipole phasing and then in monopole. The SOL density profile in the region 3.84m to 3.86m is found smaller during monopole phasing compared to dipole. This is consistent with the RF sheaths physics as the SOL density modifications are expected to be stronger when ICRF antenna straps are pulsed in phase [20]. The large error bars of the RCP measurements do not allow to make a conclusion on the impact of the ICRF power on the SOL density, however, there are some indications that the application of ICRF slightly depletes the electron density in the far SOL.

This brief account of the RF sheaths features highlights the ICRF related parameters, which are expected to have the most significant impact on the LH wave coupling: the ICRF power P_{RF} and ICRF antenna phasing.

5. EXPERIMENTAL RESULTS

5.1. EFFECT OF ICRF RELATED PARAMETERS ON LH WAVE COUPLING

The time evolution of the RCs with the applied ICRF power and the relevant plasma parameters are shown in figure 5a. The plasma configuration was such that the LHCD launcher was connected to antenna B and partially to the upper part of antenna A, figure 2a. Due to the intense gas puff and high recycling rate the electron density changes only slightly during the application of ICRF power, which helps investigating the pure effect of the ICRF power on the LH coupling. The RCs on rows #1 to #4 clearly increase with the applied power by antenna B. The RCs on the bottom two rows increase as

well but as the protection system trips the klystrons, the RC waveforms are highly irregular. When the ICRF power is turned off at 21.5s all the RCs drop below 0.1 indicating improved coupling conditions. The electron density decreases only slightly, about 5% at the core and 3% near the edge, so does the recycling, whilst the plasma limiter distance, r_{ROG}, and launcher position are kept constant. The RC change at 21.5s can be clearly related to the ICRF power. When antenna A is powered only the very bottom row shows an increase before it starts tripping again at 24.8s when the ICRF power was ramped up. These observations are in agreement with the magnetic field lines geometry and illustrate the RF sheath impact on the LH wave coupling performance.
LH wave coupling is further investigated by analysing the dependencies of the RCs in rows #1 to #6 on selected ICRF parameters: the power from antenna A and B (P_{AntA} and P_{AntB}), from straps B1-B2 (P_{B12}) and from straps B3-B4 (P_{B34}) and ICRF antenna phasings.

5.1.1 Effect of antenna A, B and B12, B34 on RC.

Direct comparison of the LH RCs with and without power from antenna B in some cases is difficult to envisage as the plasma density, which is a key factor in LH coupling performance, usually increases with the ICRF power. This has been attributed to the increase of the recycling of the hydrogenic species.

The effect of the ICRF antenna B on the LH coupling can be also validated by using one of the other ICRF antennas, e.g. antenna A, which is situated further away from the LHCD launcher and only partially connected to it, mainly at the bottom rows. The RCs during two identical JET pulses with power from antenna A and B are given in figure 5b. The plasma parameters are very similar as well as the pattern of the powered klystrons. In Pulse No: 56631 0.8MW of ICRF power was applied by the antenna B while in Pulse No: 56632 the same power was applied by antenna A. Both cases are also compared to no ICRF power references. The map of the connection lines in this case is similar to the example in figure 2a and shows that only the bottom half of the launcher is magnetically connected to antenna A, whilst the field lines cover entirely antenna B. Therefore, the substantial increase of RCs on the upper part of the launcher when pulsing with antenna B can be related to the SOL density modification by the RF sheaths. The effect of the antenna B on LH coupling is stronger on the upper two rows, which are clearly not affected by antenna A and whose RC increase about twice when applying power from antenna B. The RCs on the middle rows, i.e. rows #3, #4 and #5, increase about 1.5 times while the RC on the bottom row is the same regarding the antenna used. Antenna A has no impact on rows #1 to #5 as the corresponding RCs do not evolve compared to no ICRF power references. The geometry of nPL and PL — the former being 0.005m behind the limiters separating antennas A and B shields the local density modification less efficiently than PL — explains why antenna A does not affect row #5 in the same way as antenna B impacts on row #1. On the other side the lack of change of RC #5 and the increase of RC #6 with P_{AntA} indicates that the density pump out effect in this example is larger at the top of the antenna, Z~0.5m, compared to its extremities at Z>0.7m. The RC changes on the very bottom row are identical independently of the antenna used and taking into account nPL and PL geometry this observation means that the density depletion is larger at the top of the antenna, around Z~0.5m, compared to the middle, Z~0m.

The effect of antenna A on the LH coupling is investigated in details by analysing the RCs dependence on the applied power, P_{AntA}, and antenna phasing. The results of the RCs evolution with P_{AntA} are shown in figure 6. Black and white graphs in front of the launcher mouth display the pattern of the klystrons power, which confirms that the following cases can be compared: rows #3 and #4 in Pulse No's: 56580 and 56635 and rows #1, #2, #5 and #6 in Pulse No's: 56635 and 56634.

The RCs dependence on P_{AntA}, shows negligible effect on the upper three rows as RCs #1, #2 and #3 are not changing with P_{AntA} and this can be explained by the fact that this half of the launcher is not connected to antenna A, figure 2a. The most pronounced effect of P_{AntA} on RCs is on rows #4, #5 and #6 in dipole case. At $l_{pos} = -0.015$m the top and the bottom rows are slightly affected by P_{AntA}, whilst when the launcher is closer to the plasma, l_{pos}=-0.005m, antenna A influences mainly rows #4 and #6. In $-\pi/2$ case P_{AntA} almost does not affect the LH coupling compared to dipole case. The RC on rows #5 and #6 are larger in dipole than in $-\pi/2$ phasing.

The effect of straps B1-B2 and B3-B4, which are closer to the LHCD launcher, is investigated by pulsing them separately. The results in dipole and in $-\pi/2$ case are illustrated in figure 7. Direct comparison between Pulse No's: 56632 and 56633 can be made, as these two pulses are identical regarding the klystron configuration used. Possible evaluation between Pulse No's: 56558 and 56559 in figure 7a, however, will not be correct as seen by the different pattern of the powered klystrons.

In general ICRF straps B1-B2 and B3-B4 affect the LH coupling in a similar way. In dipole case P_{B12} does not affect the RCs on rows #1, #3, #4 and #5, while the increase of RCs with P_{B12} is larger on rows #2 and #6. RCs increase more significantly with P_{B34} as its effect is now pronounced on the middle rows as well. In $-\pi/2$ phasing rows #1 to #6 behaviour is very similar with respect to P_{B12} and P_{B34}, meaning that the two pairs B1-B2 and B3-B4 are identical from LH point of view. The only small difference in LH coupling is on rows #1 and #2 at low power from B1-B2, P_{B12} = 0.5MW in figure 7b, in which case RCs #1 and #2 are much lower than the case in which P_{B34} = 0.5MW. The quality of the coupling during no ICRF power phase confirms the substantial impact of antenna B on LHCD coupling: RCs on the upper part of the grill increase about twice, whilst the ones in the middle of the launcher rise approximately 1.5 times.

Similarly to antenna A $-\pi/2$ case, the bottom two rows are not strongly affected by P_{B12} and P_{B34}. By comparing rows #1 and #2 of all $-\pi/2$, -0.005m cases, i.e. Pulse No's: 56634 with antenna A, 56632 with straps B1-B2 and 56633 with straps B3-B4 one concludes that antenna A has no effect at all, RCs are in the range 0.06-0.08. Straps B1-B2 have effect on RCs at higher ICRF power only, P_{B12} >1MW, while at lower power levels, P_{B12}~0.5MW, this effect is negligible. Straps B3-B4 affect the RCs even at low power and RCs are the highest amongst the three cases. Row #6 shows consistent behaviour independently on the powered ICRF antenna or straps — RCs do not change with ICRF power in $-\pi/2$ cases, but always increase in dipole.

5.1.2. Effect of ICRF antenna B phasing on RC.

The ICRF antennas phasing is expected to have significant impact on the sheath magnitude and spatial distribution and consequently also on SOL density modifications. The effect of ICRF antenna phasing

is illustrated in figure 8, where the absolute values of the RCs and their increase after the application of ICRF power at four different phasings are compared.

The RCs measured at four pulses featuring similar parameters and different antenna phasings are compared in figure 8a. The highest RCs are measured on rows #1 and #2 in monopole and $-\pi/2$ phasing, whilst the RCs on the other rows do not depend strongly on the ICRF antenna phasing.

The change of the RCs, ΔRC computed as a difference between RCs during ICRF power and after its switch off, is shown in figure 8b. The plasma density in the core and at the edge has a larger increase with ICRF power in this case than in the pulse of figure 5a. Its decline of about 16% when 1.2MW of ICRF power was turned off affected the RCs so that the overall change on the middle and bottom rows was very small or even negative, which indicates improvement of the coupling with the ICRF power. In this case both contributions, plasma density and ICRF power, were correlated and acted against each other regarding the effect on the LH coupling. The relatively large amount of gas from GIM6 used during these experiments can be also responsible for the negative values on the bottom two rows. Similarly to figure 8a the change of the RCs on rows #1 and #2 is the highest for monopole and $-\pi/2$, figure 8b.

The LH wave coupling is much better when antenna B is powered in dipole and $+\pi/2$ phasing, which are mainly used at JET. In accordance with the RF sheaths physics the strongest effect on the SOL is expected in monopole phasing, while the weakest can be expected in dipole [20]. The RCs in figure 8a are consistent with this picture, i.e. the worst coupling is in monopole and better is in dipole. However, there is significant difference between $-\pi/2$ and $+\pi/2$ on row #2, which is difficult to explain. Row #6 is sensitive to the ICRF power in dipole only, shown by the small increase of RCs, figure 8b, which is consistent with the dependencies in figure 6 and figure 7.

5.1.3. Asymmetric changes of LH reflected power

In general the LH RCs increase with the ICRF power. However, under certain conditions, irregular changes of RCs over the grill mouth were observed. These mainly poloidal asymmetries can be seen in figure 8b. The reflection coefficient changes, ΔRCs, when antenna B and A are powered in dipole and $+\pi/2$ are negative on the top rows and positive during monopole and $-\pi/2$ operation. On row #5 the changes are negative with strongest impact in monopole, while ΔRCs are close to zero on row #6.

The asymmetries are displayed in plots, which show the relative increase of the reflected power, ΔP_r, on each multijunction, figure 9. It is computed according to the formula $\Delta P_r = (P_{r2} - P_{r1})/P_{r1}$, where P_{r2} and P_{r1} are the reflected power at each klystron multijunction. Figure 9 shows the detailed picture of the reflected power changes for the dipole case similar to the one shown in figure 8b. The reflected power P_{r2} was measured when 2.8MW was coupled by antenna A and B, while P_{r1} was taken when the ICRF power was switched off. The response of the multijunctions clearly shows inhomogeneous behaviour. The accuracy of this method is not very high but within two exceptions, klystrons B2 and E2 whose reflected power change is of the order of the precision of the measurements, i.e. about 0.1, two regions can be clearly identified. The central one denoted by dashed line shows predominantly smaller reflected power during the ICRF phase. The bottom

region, enclosed by dotted line, clearly shows an increase of the RCs with the ICRF power. The small toroidal differences in DP_r are due to different amount of forward and reflected power on each multijunction and the cross coupling along the rows. The peculiar values on C1 can be also due to the damage to the grill.

These dependencies suggest that ICRF antenna power induces local density modifications in JET SOL, and that in these conditions the plasma density in front of the LHCD grill is not poloidally homogeneous [8]. Similar observations have been reported by Tore Supra team as well, [25], [8].

5.2. COUPLING IN H-MODE AND USE OF GAS PUFF

5.2.1 Effect of P_{AntB} on RC in D_2 gas puffing experiments.

The LH coupling deteriorates in H-modes plasma as a consequence of the edge barrier and density depletion in the SOL. Application of ICRF power by antenna B makes the coupling in H-mode even worse. In order to improve the LHCD performance gas injection of D_2 by the near pipe GIM6 was used.

The effect of the gas puff from GIM6 was to improve significantly the coupling and to diminish the effect of P_{AntB} on the RCs. This can be seen by comparing the RCs dependence on P_{AntB} in L and H-mode, figure 10. The application of 1.3MW of ICRF power in L-mode only slightly affects the coupling, mainly on rows #2 and #3, while in H-mode none of the RCs are significantly affected when the ICRF power was increased from 0MW to 0.8 and then to 1.4MW. The coupling on row #4 is benefited by the ICRF power as the corresponding RC slightly decreases when the latter is applied. The RCs on all rows are below 0.1, which indicates good coupling conditions.

5.2.2. Improved coupling with D_2 gas puffing.

Even small amount of D_2, used in the more recent experiments, improves the coupling on the bottom three rows and larger amount improves the coupling on all rows. In H-mode using more gas provides very attractive coupling conditions, e.g. low RCs, fewer trips by the protection system and smoother power waveform, figure 11a.

The higher gas puffing rate benefits mostly the top rows, i.e. #1, #2 and #3, whilst the RCs on rows #5 and #6 increase with the gas injection rate, figure 11a, in both L and H-mode plasma. This effect was very clearly pronounced during hybrid scenario experiments, figure 11b. The increase of the RCs on the bottom rows does not necessarily indicate a decrease of the electron density in front of the launcher, in fact very steep density gradients can also lead to higher RCs. It could also be that the bottom two rows operate in an overly dense regime [5] in which RCs decrease with n_e. The density at which this occurs is estimated for JET to be around $1\times10^{18}\mathrm{m}^{-3}$ [5]. Another possible explanation of this phenomenon can be that the increase of the neutral pressure in front of these rows results in a decrease of SOL electron temperature, so that fewer electrons will have sufficient energy to ionise the D gas. If the increase of RC #5 and #6, figure 11b, is due to a density decrease and taking into account the fact that those rows are also benefiting even from a small amount of gas, ~$1\text{-}2\times10^{21}$el/s, one can suggest that there is a threshold of the gas injection rate above which the ionisation of the gas becomes slightly less efficient.

The results from gas injection studies indicate that using D_2 gas puff from GIM6 is a very promising alternative for simultaneous operation of both systems, LHCD and ICRF antenna A and B. Based on the results from the experiments on optimisation of the coupling performance, D_2 was later routinely used in JET experiments, that required power from LHCD and ICRF antennas A and B. A record of 3.4MW of LH power was coupled in H-mode, at the same time as 8MW ICRF by all antennas and 20 MW NBI, figure 12.

CONCLUSIONS

The experimental studies discussed here underline the role of the ICRF generated sheaths on the LH wave coupling.

Experiments with magnetically connected and non-connected ICRF antennas shows significant deterioration of the LHCD performance in the former case. The RCs of the rows connected to the ICRF antennas are found to increase when ICRF power is applied. This suggests that only the field line passing in the immediate vicinity of ICRF antennas are affected. The LHCD – ICRF interactions can thus be reduced on ITER by port allocation that minimises the connection between the two launching structures. The conclusions drawn after comparing different antenna phasings are consistent with the RF sheaths physics. The worst coupling was found with $-\pi/2$ and monopole phasing, whilst dipole and $+\pi/2$ phasing provided the least affected LH coupling conditions. The coupling degradation at monopole phasing is an expected consequence, however, the difference between $+\pi/2$ and $-\pi/2$ is difficult to explain.

Non homogeneous effects in the LH reflected power changes suggest that the SOL density modifications are poloidally asymmetric [8]. A density decrease or increase could be observed. Gas injection of D_2 from GIM6 is found to be a remedy for coupling improvement in H-mode plasma with ICRF power from antenna A and B at least in the range of ICRF power used.

The conclusions in the paper are also supported by SOL density measurements, according to which the application of ICRF power reduces significantly the density near the separatrix. Monopole phasing is affecting the edge density to a greater degree than dipole as confirmed by the Li beam measurements. Experimental observations are compatible with modifications of the plasma density in the SOL as described in [7]. ICRF antenna near field modelling and the effect of the new ITER like antenna on the LH coupling are foreseen as a feasible continuation of the studies.

ACKNOWLEDGEMENTS

This work was funded jointly by the United Kingdom Engineering and Physical Sciences Research Council and by the European Communities under the contract of Association between EURATOM and UKAEA. One of the authors (V.P.) was supported in part by the project GACR 202/07/0044. Discussions with D.C. McDonnald regarding the accuracy of the reflected power measurements and RCs calculations are gratefully acknowledged. The views and opinions expressed herein do not necessarily reflect those of the European Commission. This work was carried out within the framework of the European Fusion Development Agreement.

REFERENCES

[1]. Van Houtte D, *et al*, 2004, *Nucl. Fusion* **44** , L11–L15

[2]. Mailloux J, *et al*, 2002, *Phys. Plasmas* **9**, 2156

[3]. Challis C, *et al*, 2001 *Plasma Phys. Control. Fusion* **43** 861

[4]. Brambilla M, 1976, *Nucl. Fusion* **16**, 47

[5]. Litaudon X, Moreau D, 1990, *Nucl. Fusion* **30**, 471

[6]. Ekedahl A, *et al*, 2003, 15th RF Topical Conf., Moran (2003). AIP Conf. Proc. 694 (2003) 259

[7]. Becoulet M, *et al*, 2002, *Phys. Plasmas* **9**, 2619

[8]. Colas L, *et al*, 2007, *Plasma Phys. Control. Fusion* **49**, B35

[9]. Pericoli-Rudolfini V, *et al*, 2004, *Plasma Phys. Control. Fusion* **46**, 349

[10]. Kirov K K, *et al*, 2007, 17th RF Topical Conf., Clearwater (2007). AIP Conf. Proc. 933 (2007) 257

[11]. D'Ippolito D A, *et al*, 1998, *Nucl. Fusion* **38**, 1543

[12]. Pain M, *et al*, 1989, Proc. 13th Symposium on Fusion Engineering, Knoxville, Tennessee (1989)

[13]. Silva C, *et. al*, 2004, *Rev. Sci. Instrum.* **75**, 4314

[14]. Erents K, *et. al*,1985, JET report JET-P(85) 31, paper 6

[15]. Erents K, 2007, JET TF-H meeting at 25/9/2007

[16]. Korotkov A *et al*, 2004, *Rev. Sci. Instrum.* **75**, p.2590

[17]. Myra J R, *et al*, 1990, *Nucl. Fusion* **30**, 845

[18]. Myra J R, *et al*, 1996, *Phys. Plasmas* **3**, 699

[19]. D'Ippolito D A, *et al*, 1991, *Plasma Phys. Control. Fusion*, 607

[20]. D'Ippolito D A, *et al*, 1993, *Phys. Fluids B*, 3603

[21]. Riyopoulos S, 1999, *Phys Rev. E* **59**, 1111

[22]. Perkins F, 1989, *Nucl Fusion* 29, 583

[23]. Colas L, *et al*, 2005, *Nucl. Fusion* **45**, 767

[24]. D'Ippolito D A, *et al*, 2002, *Nucl. Fusion* **42**, 2357

[25]. Ekedahl A, *et al*, 17th RF Topical Conf., Clearwater (2007). AIP Conf. Proc. 933 (2007) 237

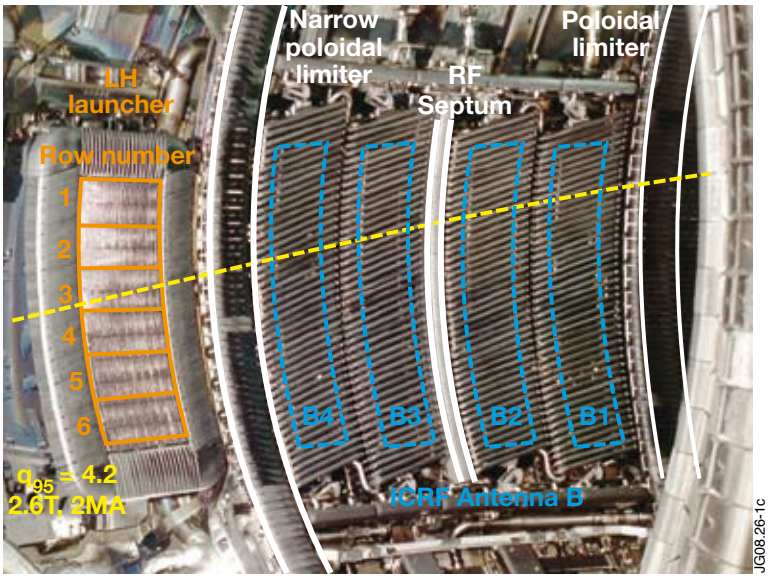

Figure 1: JET inside view showing the LHCD launcher, the ICRF antenna B separated from LHCD launcher by a narrow Poloidal Limiter (nPL), straps B1, B2, B3 and B4. A magnetic field line for typical 2.6T/2MA (q_{95}=4.2) JET pulse is mapped into the picture for illustration of the connection. The magnetic field and plasma current in all the experiments discussed here are in direction from left to right.

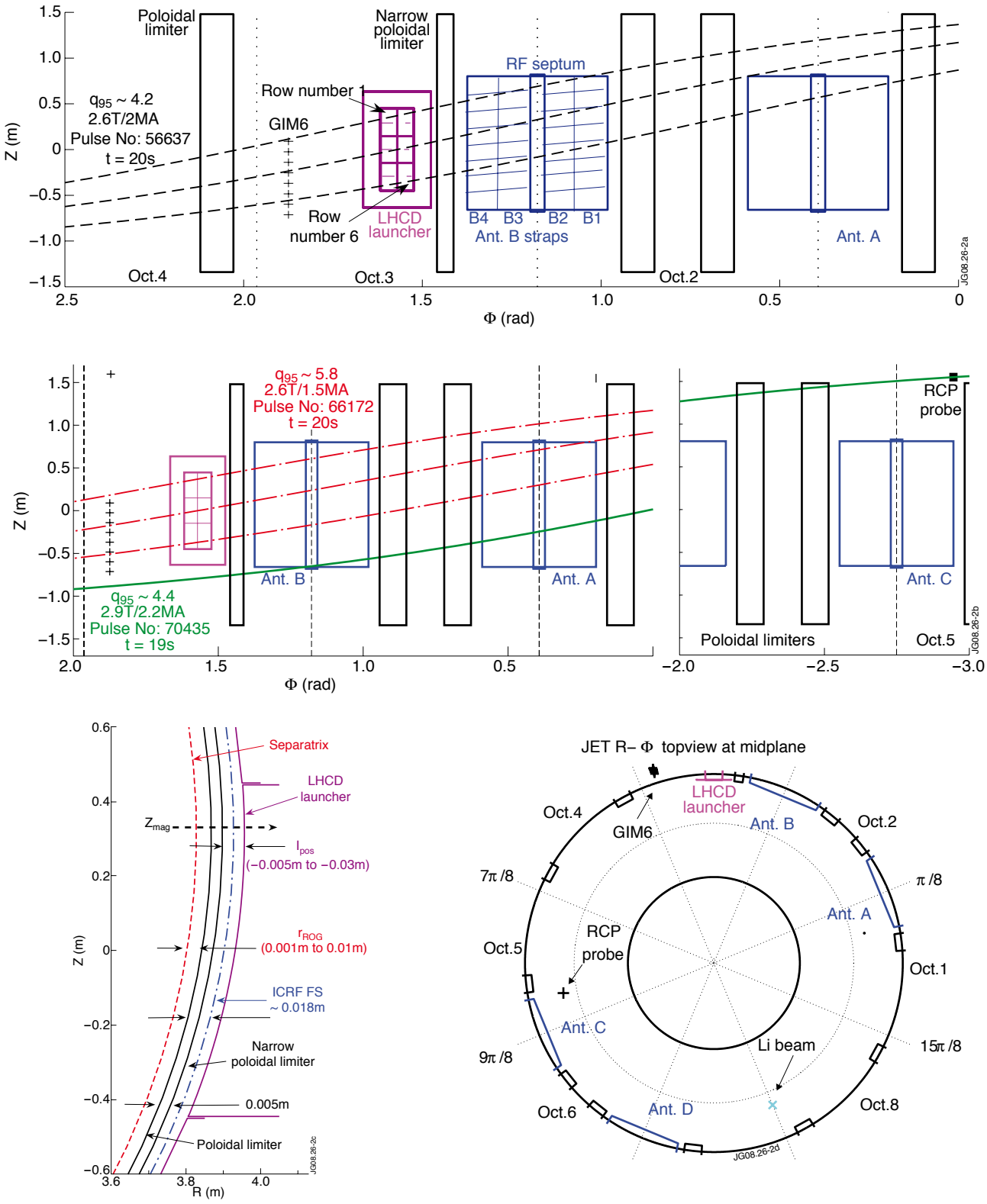

Figure 2: Φ-Z view of the LHCD launcher and near ICRF antennas in magnetic field lines in three configurations (a) and (b). A side view of the LHCD launcher showing the separatrix, the limiter and launcher profiles and the typical positions, including the distances l_{pos} and r_{ROG} is given in (c). The reference of the positive distance r_{ROG} is the PL, whilst l_{pos} is always negative as it measures the launcher position relative to nPL. The R-Φ geometry of the in-vessel components, the antennas and the approximate position of the utilised diagnostics are given in (d). Note that the ICRF antenna B screen bars and their inclination are plotted in (a) only for illustrative purpose and do not correspond to the actual ones.

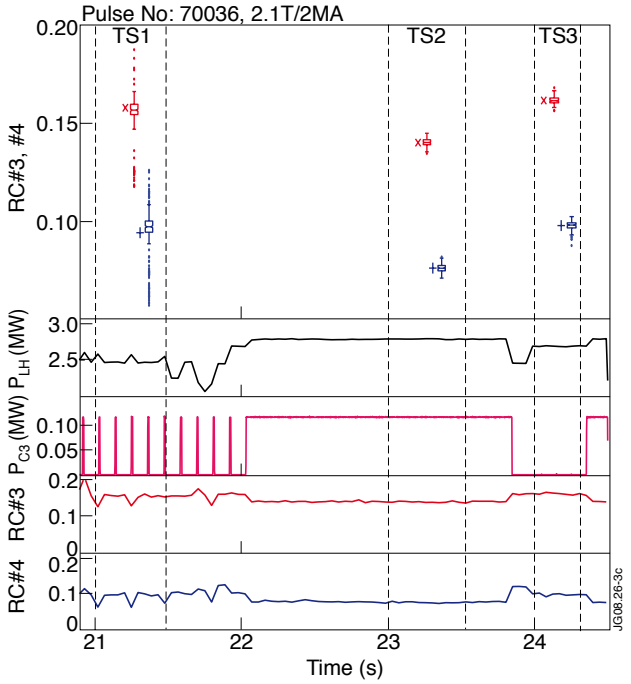

Figure 3. Statistical plots showing the distribution of the RC data in three time intervals. During the period TS1, 21s-21.5s klystrons C2, C3 and D2 were tripping. Throughout TS2, 23s-23.5s, none of klystrons was tripping and during TS3, 24s-24.3s C3 klystron was turned off. The boxes present the range in which 50% of the most likely data are, whilst the median is the horizontal line in the box. The whiskers span is about three times the standard deviation of the dataset. The dot symbols (.) show the outliers, which are the data that deviate significantly from the rest of the measurements. The measurements during TS2 and TS3 are not scattered so that the boxes are very narrow. The average values are given by (x) for RC #3 and (+) for RC #4. Below from top to bottom shown are the time evolution of the coupled LH power, P_{LH}*, the power from C3 klystron,* P_{C3}*, RC #3 and RC #4.*

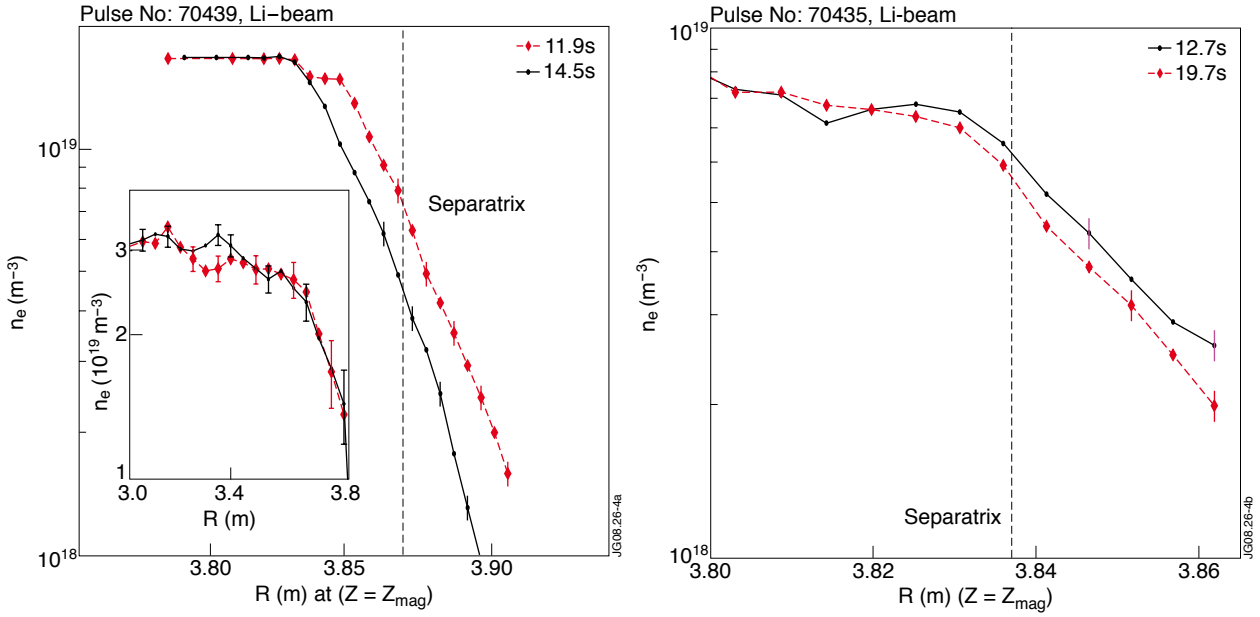

Figure 4. SOL density profiles by Li-beam diagnostic for Pulse No: 70439, 2.9T/2.2MA JET pulse (a) without RF power (11.9s, dashed line) and with 2MW of RF power (14.5s, solid line) in dipole. Core density profiles in both cases are given in the embedded graph. Density profiles for Pulse No: 70435, 2.9T/2.2MA (b) during 2.5MW of ICRF power in dipole (12.7s, solid line) and monopole (19.7s, dashed line).

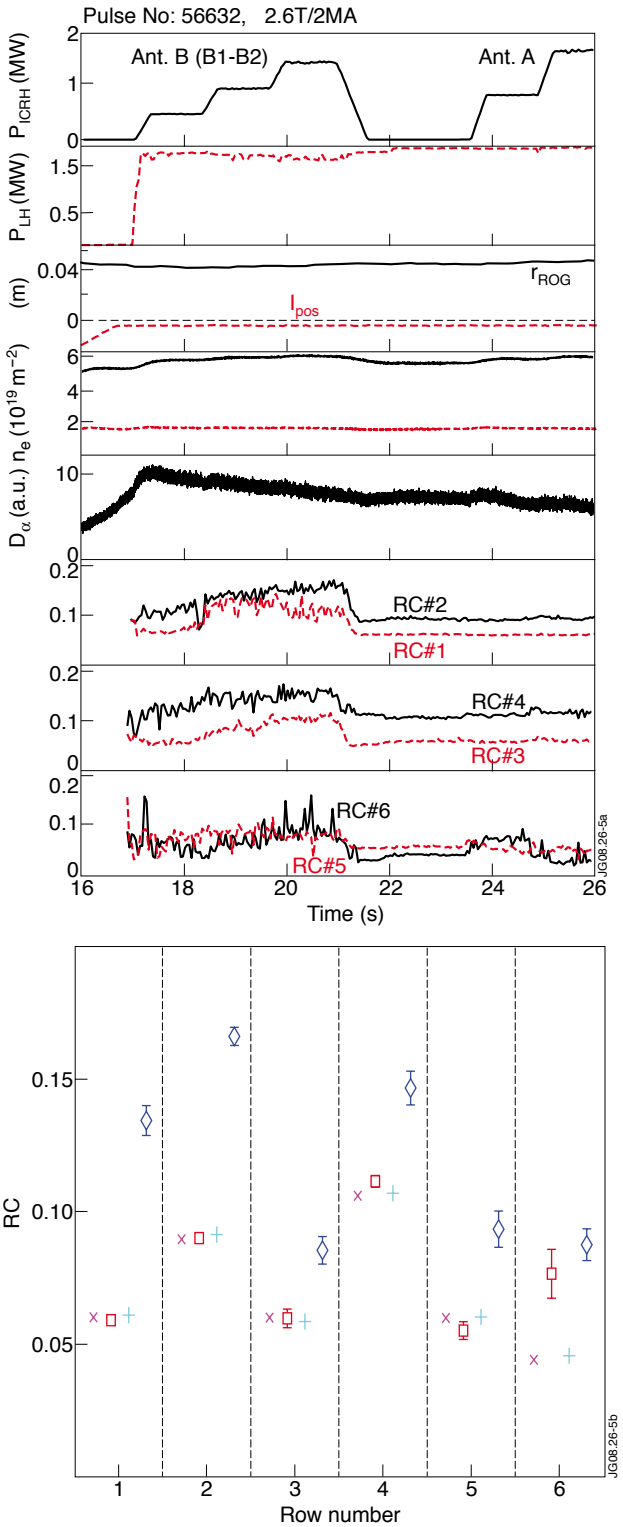

Figure 5: Effect of the ICRF antennas B and A on the LH coupling. The plasma conditions are L-mode, 2.6T/2MA, l_{pos} = −0.005m, −π/2 phasing of the ICRF antennas. From top to bottom in (a) shown are the time traces of the ICRF power, straps B1-B2 and antenna A, the LH power, the line averaged plasma density at the core (full line) and near the edge (dashed line), the recycling rate by D_α intensity, and the RCs of rows #1 to #6. The RCs are compared in (b) for two similar pulses featuring no ICRF power and 0.8MW by antenna A and B, all straps. Pulse No: 56631, 23.3s, P_{AntB}=0MW (+) and 24.4s, P_{AntB}=0.8MW (◇) and Pulse No: 56632, 23.3s, P_{AntA}=0MW (×) and 24.4s, P_{AntA}=0.8MW (□).

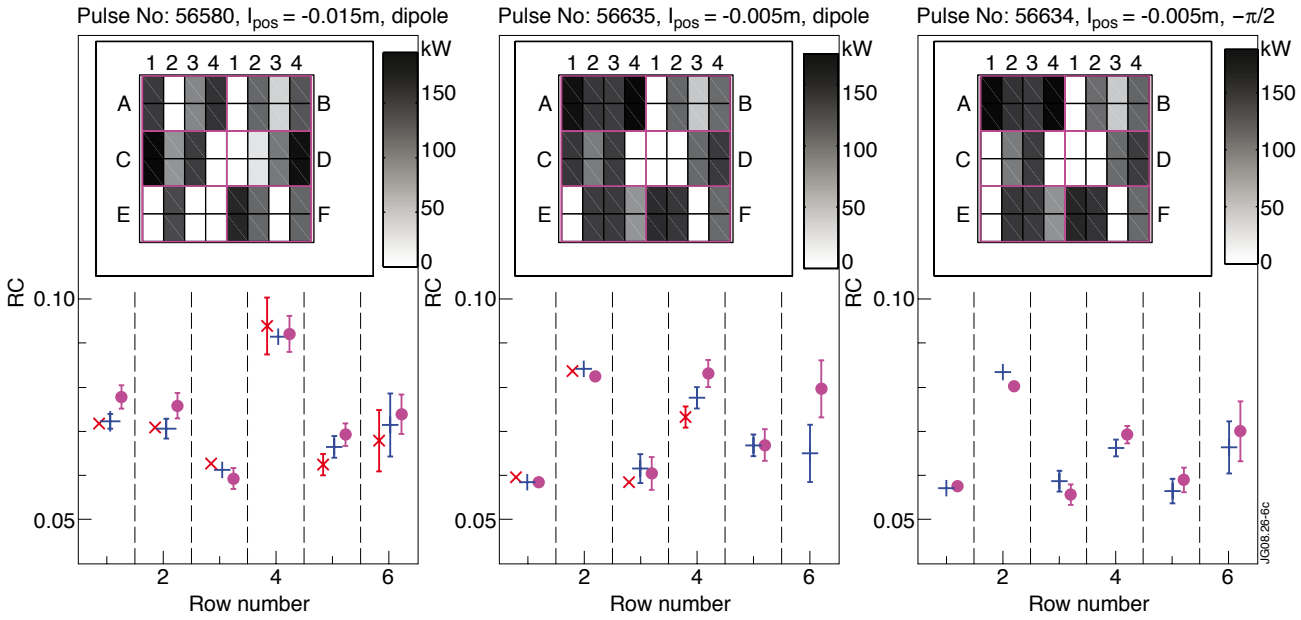

Figure 6: Antenna A effect on the LH RCs at different launcher positions (Pulse No's:56580, l_{pos}=-0.015m; 56634 and 56635, l_{pos}= -0.005m), and at different ICRF antenna phasing (Pulse No's: 56580 and 56535, dipole; 56634, −π/2). ICRF coupled power by antenna A in all the three 2.6T/2MA JET pulses is P_{AntA}=0.9MW(×), P_{AntA}=1.8MW(+) and P_{AntA}=2.6MW (.). The pattern of the powered klystrons is shown in incorporated plots as well.

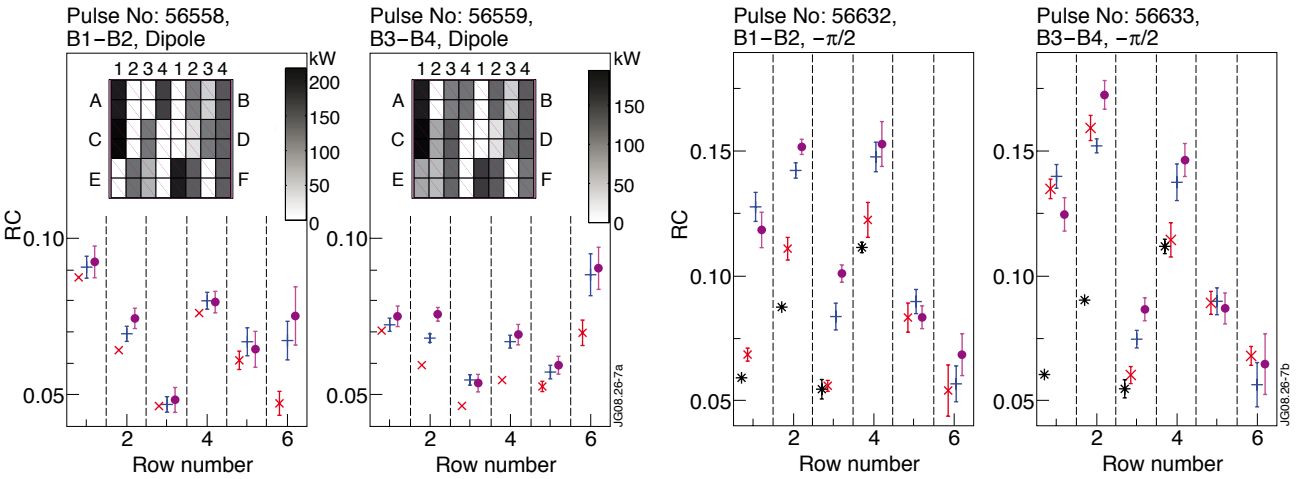

Figure 7: Effect of ICRF antenna B straps B1-B2 and B3-B4 on LH coupling. L-mode, 2.6T/2MA, l_{pos}=-0.005m, no gas puff and (a) Pulse No's: 56558 B1-B2 and 56559 B3-B4 in dipole P_{B12}=P_{B34}=0.4MW (×), P_{B12}=P_{B34}=0.8MW (+), P_{B12}=P_{B34}=1.3MW (·) and (b) Pulse No's: 56632 B1-B2 and 56633 B3-B4 in −π/2 P_{B12}=P_{B34}=0MW (*), P_{B12}=P_{B34}=0.5MW (x), P_{B12}=P_{B34}=1.0MW (+), P_{B12}=P_{B34}=1.5MW (·). The pattern of the klystrons power is shown in (a) only as the two cases in (b) are identical.

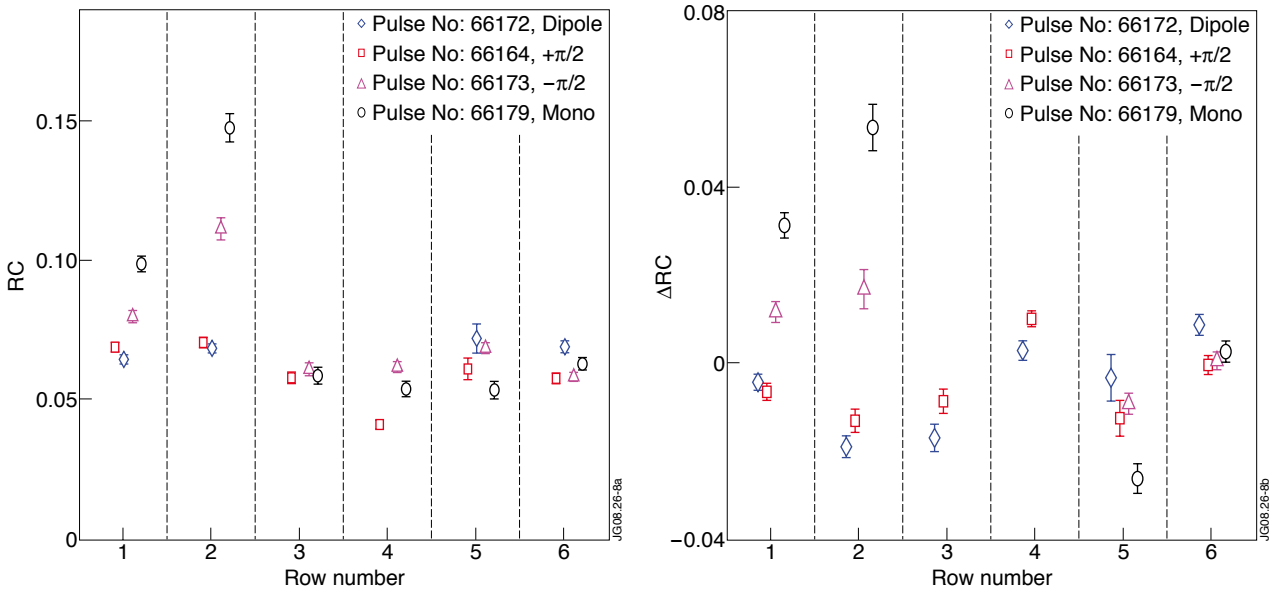

Figure 8: The RCs on rows #1 to #6 (a) and their change (b) after application of 1.2MW ICRF power in +π/2, dipole, -π/2 and mono phasings of the ICRF antennas. L-mode plasma, 2.6T/1.5MA, l_{pos} ~ -0.025m, and D_2 gas, equivalent electron rate during the puff from GIM6, $R_{GIM6} \sim 6.5\times10^{21}$ el/s, was used.

$\Delta P_r = (P_{r2} - P_{r1})/ P_{r1}$, (a.u.)
P_{r1} (Pulse No: 66172, 21.5-21.6s)
P_{r2} (Pulse No: 66172, 19.3-19.8s)

	1	2	3	4	1	2	3	4	
A	X	0.0	X	0.0	X	0.1	−0.1	0.0	B
	X	−0.2	−0.2	0.0	−0.3	0.1	−0.1	−0.3	
C	0.1	0.0	−0.2	X	−0.1	−0.3	X		D
	X	0.0	0.4	0.0	0.0	X	0.1		
E	0.1	−0.1							F
	0.4	0.1							

JG08.26-9c

Figure 9: Non-homogeneous effect of the ICRF power on the LH coupling. The numbers in the boxes indicate the relative increase of the reflected power ΔP_r computed as $\Delta P_r = (P_{r2} - P_{r1}) / P_{r1}$ where P_{r2} and P_{r1} are the reflected powers in two cases. The empty boxed correspond to unused klystrons, whilst the 'X' sing shows the ones for which the reflected power changes are within the error bars of the measurement. JET Pulse No: 66172 is compared with and without ICRF power while plasma parameters, configuration and the pattern of the powered klystrons are identical in both cases.

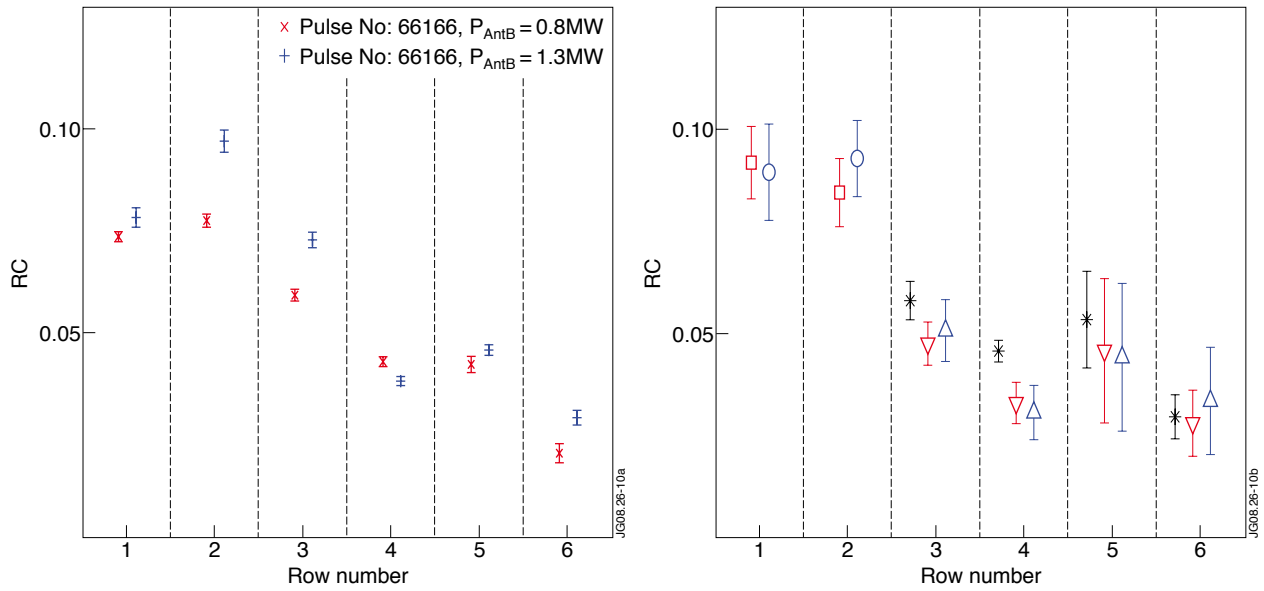

Figure 10: LH coupling at different P_{AntB} *in L (a) and H-mode (b) plasma. 2.6T/1.5 MA,* D_2 *puffing from GIM6 was used, equivalent electron rate,* $R_{GIM6} \sim 4.5\times10^{21}$ *el/s, ICRF power by antenna B+A in* $+\pi/2$ *phasing,* l_{pos}*=-0.025m in (a) and –0.03m in (b), Pulse No's: 66166,* P_{AntB}*=0.6MW (∇); 66161,* P_{AntB}*=0.8MW ( ); #66171,* P_{AntB}*=0MW (*),*

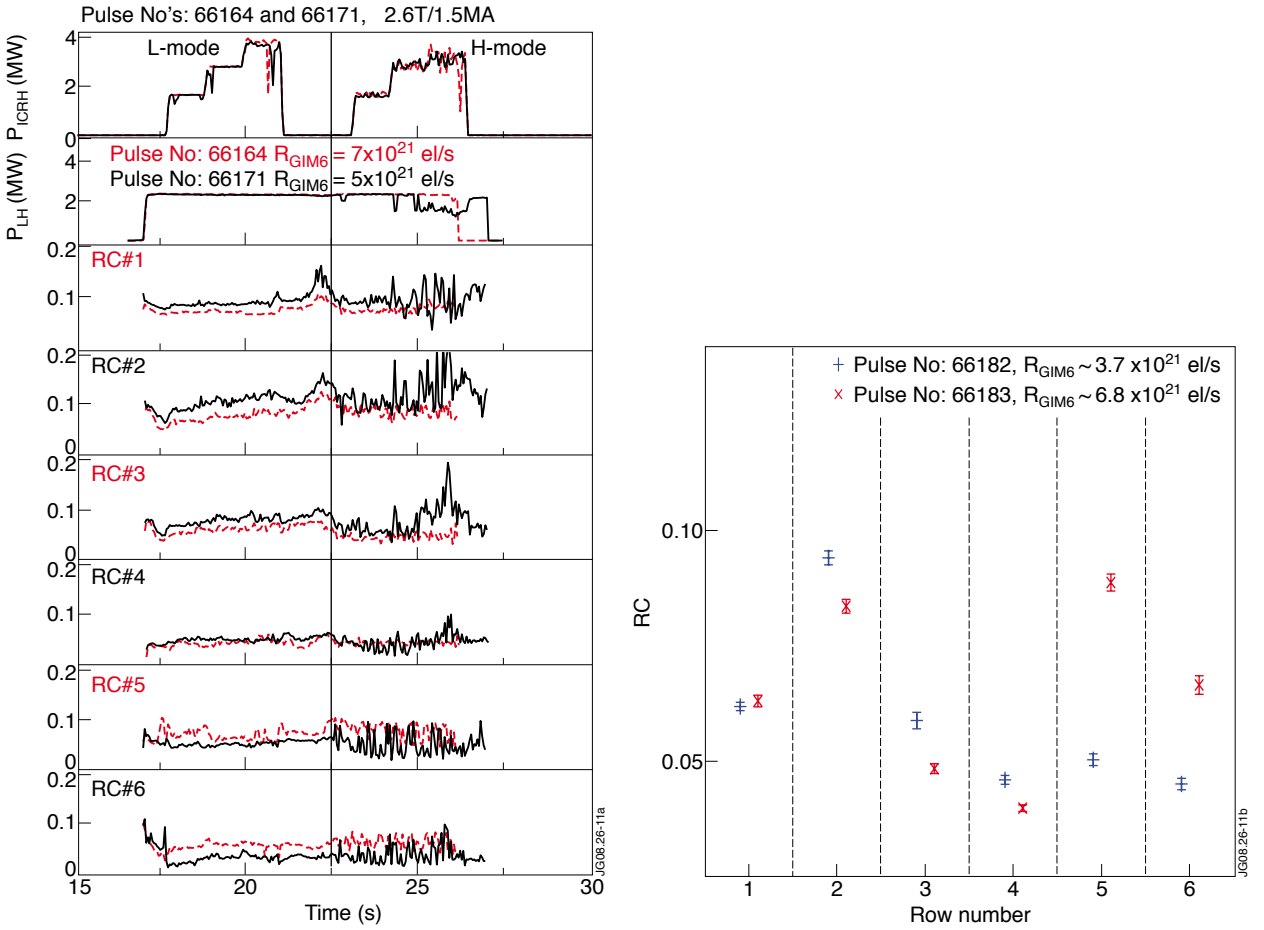

Figure 11: Time traces (a) of two similar JET pulses with low (solid line) and high (dashed line) D_2 *gas puff rate. Ant. B+A in* $+\pi/2$ *phasing and* l_{pos} *= –0.025m in L and –0.03m in H-mode. RCs dependence (b) on the near launcher gas injection rate by GIM6. 3.1T/2.3MA H-mode plasma, 1.2MW of ICRF power by antenna A and B in dipole and* l_{pos}*=–0.025m. The equivalent electron rate during* D_2 *gas puff from GIM6,* R_{GIM6}*, is indicated in the legends.*

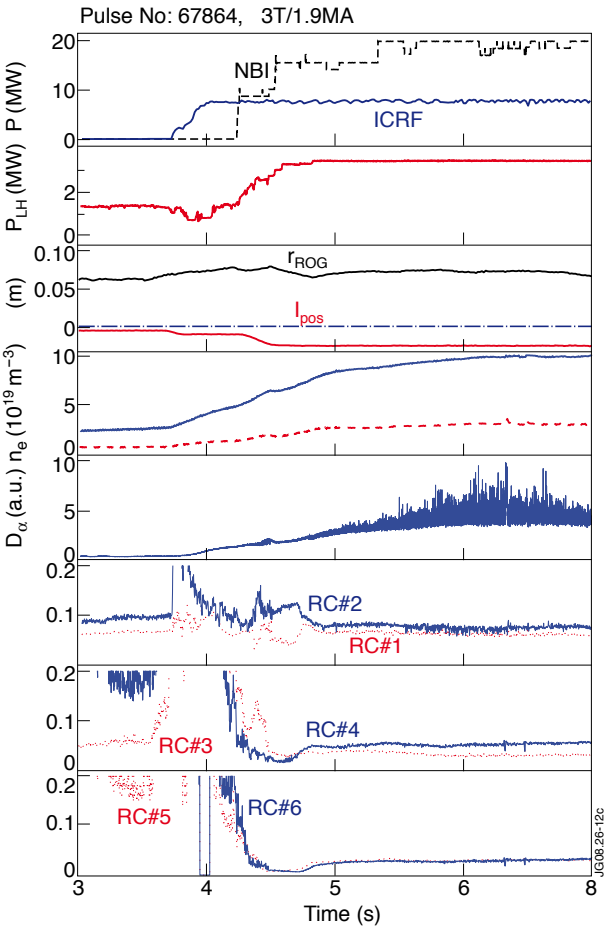

Figure 12: JET Pulse No: 67864, 3T/1.9MA, H-mode, 3.8×10^{21}el/s D2 puff from GIM6 was introduced from 3.5s until the end of the LHCD power. From top to bottom the time traces are as follow: NBI (dashed line) and ICRF power (solid line), the LH power, r_{ROG} and l_{pos}, line averaged plasma density at the core (solid line) and near the edge (dashed line), D_a intensity, and the RCs of rows #1 to #6.